Archives of Biochemistry and Biophysics 762 (2024) 110176

Contents lists available at ScienceDirect

Archives of Biochemistry and Biophysics

journal homepage: www.elsevier.com/locate/yabbi

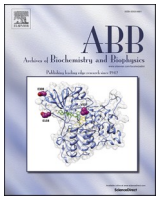

# Folic acid-functionalized and acetyl-terminated dendrimers as nanovectors for co-delivery of sorafenib and 5-fluorouracil

Ali Hussein Mezher, Mahboobeh Salehpour *, Zohreh Saadati **

*Department of Chemistry, Omidiyeh Branch, Islamic Azad University, Omidiyeh, Iran*

ARTICLE INFO

*Keywords:*
Dendrimers
Sorafenib
5-Fluorouracil
Co-delivery
MD simulations

ABSTRACT

Molecular dynamics (MD) simulations were employed to investigate the simultaneous association of sorafenib (SF) and 5-fluorouracil (5-FU) with generation 4 (G4) acetyl-terminated poly(amidoamine) (PAMAM) dendrimers conjugated with folic acid (G4ACE-FA). Simulations were conducted under physiological (pH 7.4) and acidic (pH < 5) conditions, representing the environments of healthy and cancerous cells, respectively. The average radius of gyration ($R_g$) of G4ACE-FA was determined to be approximately 1.85 ± 0.01 nm and 2.31 ± 0.03 nm under physiological and acidic conditions, respectively. Drug loading did not exert a significant influence on the size and conformational compactness of G4ACE-FA at both neutral and low pH. However, a discernible increase in dendrimer size was observed upon simultaneous encapsulation and/or conjugation of both drug molecules. The relaxation times of G4ACE-FA were calculated to be 10.2 ns and 9.6 ns at neutral and low pH, respectively, indicating comparable equilibrium rates under both pH environments. The incorporation of small 5-FU molecules did not demonstrably alter the dendrimer's microstructure. The observed doubling of the relaxation time under acidic conditions can be attributed to the relatively compact structure of the dendrimer at neutral pH and the continuous intrastructural rearrangements occurring at acidic pH. The prolonged relaxation time observed in the G4ACE-FA:5-FU:SF complex is attributed to competitive interactions between 5-FU and SF molecules during simultaneous encapsulation by the dendrimer. Analysis of the unloaded and loaded structures of G4ACE-FA under varying pH conditions revealed a densely packed conformation at neutral pH and a more open, sponge-like structure at low pH. The solvent-accessible surface area (SASA) of the dendrimer was assessed at both pH conditions. At neutral pH, SASA values were approximately 124.0 ± 2.8 $nm^2$, 127.5 ± 2.6 $nm^2$, 131.3 ± 2.6 $nm^2$, and 133.3 ± 2.6 $nm^2$ for unloaded G4ACE-FA and the G4ACE-FA:5-FU, G4ACE-FA:SF, and G4ACE-FA:5-FU:SF complexes, respectively. Drug incorporation had a minimal effect on SASA at neutral pH. At low pH, the corresponding values were 198.2 ± 4.7 $nm^2$, 195.8 ± 4.8 $nm^2$, 212.5 ± 6.1 $nm^2$, and 215.4 ± 4.2 $nm^2$. These findings suggest that 5-FU encapsulation resulted in minimal changes to the dendrimer's surface exposure to the solvent, potentially due to its small size. In contrast, SF interaction led to a more pronounced increase in SASA, indicating structural expansion to accommodate SF conjugation. The equilibrium stoichiometry of the G4ACE-FA:5-FU complex was determined to be 1:11 and 1:3 at neutral and low pH, respectively. Similarly, the G4ACE-FA:SF complex exhibited equilibrium stoichiometries of 1:10 and 1:4 at neutral and low pH. The G4ACE-FA:5-FU:SF complex displayed stoichiometries of 1:11:10 at neutral pH and 1:3:3 at low pH. Collectively, these findings suggest that G4ACE-FA holds promise as a versatile nanovector capable of tightly binding drug molecules at neutral pH and facilitating their release within tumor cells, thereby enabling targeted drug delivery. Furthermore, the co-loading of 5-FU and SF did not compromise the loading capacity of G4ACE-FA. At neutral pH, 5-FU molecules were distributed evenly across the dendrimer surface and within its cavities, with 6 molecules encapsulated internally and 5 conjugated on the surface. At low pH, all bound 5-FU molecules were located at the dendrimer periphery. Similarly, at neutral pH, SF molecules were found both internally (6 molecules) and on the surface (4 molecules). At low pH, 2 SF molecules were found on the surface and 2 were internally complexed. The preferred binding sites of 5-FU and SF remained largely unchanged when co-loaded onto the dendrimer. This suggests that co-delivery of 5-FU and SF using G4ACE-FA could be a promising strategy for enhancing the therapeutic efficacy of these chemotherapeutic agents.

* Corresponding author.
** Corresponding author.
*E-mail addresses:* ali.unido@gmail.com (A.H. Mezher), Ma.salehpour@iau.ac.ir (M. Salehpour), Zo.saadati@iau.ac.ir (Z. Saadati).

https://doi.org/10.1016/j.abb.2024.110176
Received 19 May 2024; Received in revised form 5 September 2024; Accepted 7 October 2024
Available online 10 October 2024

## 1. Introduction

The development of effective and targeted drug delivery systems is essential in the field of medicine to improve the efficacy and reduce the side effects of anticancer drugs. Among the promising nanocarriers, dendrimers have emerged as a popular choice due to their well-defined structure, high drug-loading capacity, and ability to encapsulate different therapeutic agents. Acetyl-terminated (ACE) polyamidoamine (PAMAM) dendrimers are particularly useful in targeted drug delivery applications and offer several advantages. These dendrimers can be designed to control drug release kinetics, have a high density of functional groups on their surface, enhance the stability and solubility of drugs, facilitate specific recognition and binding to overexpressed receptors on cancer cells, exhibit low toxicity, and promote cellular uptake of the drug-loaded dendrimer nanoparticles. By modifying the dendrimer structure, researchers can tailor the drug release profile to achieve sustained or triggered release of the encapsulated drug at the target site. The high drug-loading capacity of PAMAM dendrimers can enhance the therapeutic efficacy of the drug delivery system by delivering a higher concentration of the drug to the target tissue. Dendrimers can also encapsulate hydrophobic drugs within their interior cavities, improving the solubility and stability of poorly water-soluble drugs. This property is particularly beneficial for enhancing the bioavailability and pharmacokinetic properties of hydrophobic anticancer drugs. Targeting ligands such as folic acid, antibodies, or peptides can be added to acetyl-terminated PAMAM dendrimers to facilitate specific recognition and binding to overexpressed receptors on cancer cells. This targeted delivery approach enhances the accumulation of the drug at the tumor site while minimizing off-target effects on healthy tissues. PAMAM dendrimers are biocompatible materials that exhibit low toxicity when properly designed and functionalized. The use of acetyl-terminated dendrimers reduces the potential for cytotoxicity, making them suitable carriers for drug delivery applications. The cationic nature of PAMAM dendrimers promotes interactions with negatively charged cell membranes, facilitating cellular uptake of the drug-loaded dendrimer nanoparticles. Overall, acetyl-terminated PAMAM dendrimers offer a versatile platform for targeted drug delivery with customizable properties that can be tailored to meet specific therapeutic requirements. Their unique characteristics make them valuable tools for enhancing the efficacy and safety of anticancer drug delivery systems [1–3]. Conjugating folic acid with nanocarriers of anticancer drugs presents several benefits in targeted drug delivery applications, particularly in cancer therapy. Folate receptors are often overexpressed on the surface of many types of cancer cells, making them attractive targets for selective drug delivery. Researchers can exploit several advantages by incorporating folic acid onto the surface of nanocarriers, such as PAMAM dendrimers. Firstly, the targeting of cancer cells becomes more precise, thanks to the folic acid's ligand that specifically binds to folate receptors overexpressed on cancer cells. This process enables the drug delivery system to target tumor cells specifically, while sparing healthy tissues, thereby minimizing off-target effects and reducing systemic toxicity. Secondly, the cellular uptake of the encapsulated drug within the tumor cells increases, thanks to folate receptor-mediated endocytosis. This mechanism enhances the therapeutic efficacy of the anticancer treatment. Thirdly, folate receptor-mediated delivery can improve the pharmacokinetic properties of the drug by increasing its retention time at the tumor site. This prolonged exposure to the drug leads to higher intracellular drug concentrations and improved antitumor effects. Fourthly, folate receptor-targeted drug delivery systems can potentially overcome multidrug resistance mechanisms in cancer cells. This process enhances the sensitivity of cancer cells to the treatment by delivering chemotherapeutic agents directly to the tumor cells through folate receptor-mediated uptake, bypassing efflux pumps and other resistance mechanisms. Fifthly, folate receptor-targeted drug delivery systems offer a personalized medicine approach by tailoring the treatment to individual patients based on their folate receptor expression levels. This precision medicine strategy can optimize therapeutic outcomes and minimize adverse effects in cancer patients. Lastly, folic acid-conjugated nanocarriers can deliver a combination of drugs or therapeutic agents to target multiple pathways involved in cancer progression. This synergistic approach can enhance the efficacy of anticancer treatments and overcome drug resistance mechanisms, leading to improved patient outcomes. In summary, conjugating folic acid with anticancer drug nanocarriers provides a targeted and efficient strategy for delivering therapeutic agents specifically to cancer cells with high folate receptor expression. This approach holds great promise for enhancing the effectiveness of anticancer therapies while minimizing side effects associated with conventional chemotherapy [4–8]. In Table 1, a comprehensive overview is presented, detailing both experimental and theoretical investigations conducted on folic acid-conjugated nanocarriers within the realm of drug delivery.

5-Fluorouracil (5-FU) and Sorafenib (SF) are two commonly used anticancer drugs with distinct mechanisms of action and applications in cancer therapy [9–11]. 5-FU is a chemotherapeutic agent often used to treat solid tumors such as colorectal, breast, and head and neck cancers. It works by inhibiting thymidylate synthase, an enzyme essential for DNA synthesis, and disrupting DNA replication. As a result, it induces cell cycle arrest and apoptosis in rapidly dividing cancer cells. However, it can cause severe side effects, including gastrointestinal issues such as nausea, vomiting, diarrhea, myelosuppression, mucositis, and dermatological reactions [12,13]. SF is a multi-kinase inhibitor approved for the treatment of advanced hepatocellular carcinoma (liver cancer) and renal cell carcinoma. SF inhibits multiple kinases involved in tumor growth and angiogenesis, including RAF kinase, VEGFR, and PDGFR. By targeting these pathways, Sorafenib suppresses tumor proliferation and angiogenesis. Common side effects of SF include hand-foot skin reaction, diarrhea, hypertension, fatigue, and liver toxicity [14,15]. Utilizing nanocarriers for 5-FU and SF delivery can improve their solubility, stability, and bioavailability. Nanocarriers can also enhance the selective accumulation of these drugs in tumor tissues while minimizing off-target effects on healthy tissues. Additionally, nanocarriers can help overcome the limitations of SF's poor water solubility and potential drug resistance mechanisms. In conclusion, 5-FU and SF are important anticancer drugs with specific mechanisms of action and applications in cancer therapy. The use of nanocarriers for the delivery of these drugs offers significant advantages in improving their therapeutic outcomes by enhancing targeting specificity, reducing side effects, and overcoming drug resistance. By encapsulating 5-FU and SF within nanocarriers, researchers can optimize the delivery of these drugs to tumor sites, leading to improved treatment efficacy and patient outcomes in cancer therapy.

MD simulations offer a powerful tool for investigating drug delivery systems at the molecular level, providing valuable insights into drug-nanocarrier interactions, permeation mechanisms, and resistance mechanisms. By leveraging the predictive capabilities of MD simulations, researchers can accelerate the development of innovative drug delivery systems with improved targeting specificity, enhanced bioavailability, and reduced side effects, ultimately advancing the field of drug delivery and personalized medicine. Our study investigates the potential of using G4ACE-FA for the simultaneous delivery of 5-FU and SF to tumor cells. Through all-atom molecular dynamics (MD) simulations, we aim to gain insights into the interactions between the dendrimer-based drug delivery system and the tumor cell membrane at the atomic level. By understanding the molecular mechanisms governing the drug release and uptake processes, we seek to optimize the design of the dendrimer carrier for enhanced therapeutic efficacy.

This research holds great promise for advancing the field of cancer therapy by providing a deeper understanding of the complex interplay between nanocarriers and biological systems. Ultimately, our findings may pave the way for developing more efficient and targeted drug delivery strategies for combating cancer.

**Table 1**
Brief description of the reviewed papers' aim, methods, and significant results and conclusions.

| Author(s) | Year | Research Focus/Methodology | Key Findings/Results |
|---|---|---|---|
| Badalkhani-Khamseh et al. [1] | 2017 | This study, using fully atomistic MD simulations, investigated the association of 5-Fluorouracil (5-FU) with amine ($NH_2$) and hydroxyl (OH)-terminated PAMAM dendrimers of generations 3 and 4 (G3 and G4). | The study determined the stoichiometry of the formed complexes, revealing a 1:12, 1:1, 1:27, and 1:4 ratio for G3$NH_2$-FU, G3OH-FU, G4$NH_2$-FU, and G4OH-FU, respectively. These results align with experimental isothermal titration calorimetry data. The surface chemistry of PAMAM dendrimers significantly influences their drug-loading capacity and the location of drug molecules within the dendrimer structure. While amine-terminated dendrimers offer higher drug encapsulation due to their open structure, hydroxyl-terminated dendrimers provide a different drug-binding environment due to their dense structure and surface-localized interactions. |
| Badalkhani-Khamseh et al. [2] | 2018 | This study aimed to investigate the interaction behavior of Chalcone (CHL) with PAMAM dendrimers possessing different surface functional groups (amine, carboxyl, and acetyl) at both neutral and low pH conditions. | At neutral pH, PAMAM dendrimers adopt a densely packed structure, encapsulating CHL primarily through nonpolar interactions. At low pH, G4-AMN and G3.5-ACE exhibit a more open architecture with larger cavities. G4-ACE retains a more compact structure with smaller cavities, keeping CHL closer to the surface.<br>At neutral pH, CHL interacts strongly with G4ACE, suggesting a stable complex suitable for drug delivery in the human body. The interactions are primarily nonpolar (van der Waals and hydrophobic) at neutral pH.<br>CHL is most difficult to release from G4ACE due to its compact structure. This suggests that G4ACE could be ideal for controlled drug release.<br>At low pH, the energy barrier for CHL release is significantly lower for all dendrimers (1.9–2.7 kcal.mol$^{-1}$), indicating that the drug could be released more readily under acidic conditions. |
| Tu et al. [3] | 2023 | This study focused on investigating the structural properties of fatty-acid (FTA) modified PAMAM dendrimers using coarse-grained molecular dynamics (CGMD) simulations. | Dendrimer size and structure are influenced by generation, fatty acid chain length, and pH.<br>At low pH (5), protonation of interior amines leads to FTA chain localization on the dendrimer surface. At higher pH (7), FTA chains tend to aggregate within the dendrimer's interior, causing crowding.<br>Higher grafting density and longer fatty acid chains likely contribute to more pronounced structural changes.<br>The hydrophobic nature introduced by FTA chains could potentially enhance drug loading, while the controlled structural changes based on pH could be exploited for targeted drug release.<br>The hydrophobically modified dendrimers hold promise for reduced toxicity. |
| Shafi Ullah et al. [7] | 2022 | This study focused on developing and characterizing folic acid-modified chitosan nanoparticles loaded with 5-fluorouracil (5-FU) for targeted drug delivery to colon cancer cells. | Successful synthesis and characterization of folic acid-modified chitosan nanoparticles (FA–CS–5FU-NPs) was confirmed using FTIR and NMR spectroscopy.<br>The nanoparticles were monodispersed with an acceptable size (235 $\pm$ 12 nm), positive surface charge (+20 $\pm$ 2 mV), and good drug entrapment efficiency (59 $\pm$ 2 %).<br>In vitro drug release studies demonstrated the controlled release of 5-FU. FA–CS–5FU-NPs exhibited significantly higher cytotoxicity against colon cancer cells compared to CS-5FU-NPs, indicating that folic acid targeting improved drug delivery to cancer cells. |
| Demirel et al. [8] | 2020 | This study focused on developing and characterizing folic acid-conjugated, pH and redox-sensitive hybrid magnetic nanoparticles for targeted and triggered drug delivery. | The authors designed pH- and redox-triggered magnetic lipid-polymer hybrid nanoparticles (MHNPs) with a core-shell structure.<br>Dual-triggered drug release was achieved in response to specific stimuli. Folic acid-MHNPs loaded with doxorubicin (FA-MHNPs-DOX) exhibited efficient drug release at an acidic pH (5.5) and in the presence of glutathione (10 mM), mimicking the conditions found in the tumor microenvironment.<br>Folic acid conjugation enhanced cellular uptake and cytotoxicity. FA-MHNPs-DOX showed significantly improved cellular uptake and cytotoxicity against breast cancer cells compared to non-targeted MHNPs-DOX.<br>FA-MHNPs-DOX induced apoptosis in breast cancer cells. The nanoparticles effectively reduced cell viability and triggered apoptosis in the targeted cancer cells. |
| Yahyavi et al. [13] | 2023 | This study used molecular dynamics simulations to investigate the potential of folic acid (FA) functionalized carbon nanotubes (CNT) as pH-responsive carriers for the anticancer drug fluorouracil (5-FU). | FA functionalization does not significantly affect the initial drug loading capacity of CNT at neutral pH. Both CNT and CNTFA can load approximately 51 5-FU molecules.<br>CNTFA exhibits pH-responsive drug-release behavior. While CNTFA retains a high drug loading capacity at neutral pH, the loading capacity decreases to 45 molecules at low pH.<br>Hydrophobic and $\pi$-$\pi$ stacking interactions are the primary forces stabilizing the CNTFA-5-FU complex.<br>Drug release is thermodynamically favored at low pH. The binding free energy is lowest for CNTFA:5-FU at low pH, indicating a higher propensity for drug release under acidic conditions.<br>Diffusion coefficients suggest tighter drug binding at neutral pH and enhanced release at low pH. The diffusion coefficient of 5-FU is lower at neutral pH, implying that the drug is tightly bound to CNTFA, while it is higher at low pH, indicating enhanced drug release. |

## 2. Computational details

The initial structural models of generation 4 (G4) acetyl-terminated poly(amidoamine) (PAMAM) dendrimers (G4ACE) were constructed using GaussView 5.0 software [16]. The G4ACE-FA system, representing the folic acid (FA)-conjugated dendrimer, was parameterized for both neutral and acidic pH conditions using the AMBER99SB force field [17]. This force field encompassed both bonded interactions (bond lengths, bond angles, dihedral, and improper angles) and nonbonded interactions (electrostatic and van der Waals forces). To accurately represent the charge distribution across the dendrimer, the PAMAM structure was conceptually partitioned into three distinct regions: (1) the central ethylenediamine core, (2) the branching monomers comprising the dendrimer's architecture, and (3) the terminal units at the dendrimer's periphery. Each of these regions underwent optimization using the B3LYP functional and the 6-31G(d) basis set within the Gaussian 09 software package [18]. Subsequently, partial atomic charges were assigned to each atom using the restrained electrostatic potential (RESP) method, facilitated by the PyRED server [19]. Guided by experimental findings [20], a 39 % surface functionalization with FA molecules was implemented. This translated to the random conjugation of 25 FA molecules to the acetyl-terminated surface groups of the G4ACE dendrimer. The bonded and nonbonded parameters for FA, sorafenib (SF), and 5-fluorouracil (5-FU) were meticulously calculated using the Antechamber software [21]. The resulting coordinate and topology files were subsequently converted into a format compatible with the GROMACS simulation package using ACPYPE software [22]. All-atom molecular dynamics (MD) simulations were conducted using the GROMACS 5.1 package [23], with the VMD 2.9 program serving as a visualization tool [24]. As follows from potentiometric (acid-base) titrations, the p$K_a$ value of primary and tertiary amines of $NH_2$-terminated PAMAM dendrimers at physiological pH is about 9.50 [25–27] and 6.50 [28], respectively. Thus, at neutral pH, the primary amines of the surface groups become protonated [29]. However, at lower pH values, the tertiary amines within the dendrimer's branching structure also undergo protonation. Since the peripheral amines in G4ACE are substituted with acetyl groups, they remain uncharged. This crucial aspect was meticulously incorporated into the simulation protocols to accurately replicate the acidic pH conditions characteristic of the tumor microenvironment. Folic acid molecules exhibit a charge of −1 at physiological pH and 0 at acidic pH. Consequently, the net charge of the G4ACE-FA dendrimer at neutral and low pH was calculated to be −25 and + 62, respectively. The bonded and nonbonded parameters for 5-FU and SF were determined using the same methodology employed for FA. The p$K_a$ values for 5-FU range from 7.76 to 8.02 [29], indicating that protonated and doubly protonated forms are not observed within the pH range of 0–14. Under pH conditions below and above 8.0, 5-FU exists in its neutral and singly deprotonated forms, respectively [30]. In contrast, SF carries a charge of 0 at neutral pH and +1 at acidic pH. To initiate the MD simulations, all-atom MD simulations of the G4ACE-FA dendrimer were performed at both neutral and acidic pH conditions. These equilibrated structures then served as the starting configurations for subsequent dendrimer-ligand simulations. Short-range nonbonded interactions were modeled using the 12-6 Lennard-Jones potential with a cutoff distance of 12 Å. Periodic boundary conditions were implemented in all spatial directions, and the Particle Mesh Ewald (PME) method was employed to accurately calculate long-range electrostatic interactions.

Cubic solvation boxes were constructed using the TIP3P water model, with a 10 Å solvation shell surrounding the dendrimer to ensure adequate hydration. A salt concentration of 0.145 M ($Na^+Cl^-$) was incorporated into all systems, providing a more realistic representation of physiological conditions. The steepest descent minimization algorithm, followed by the conjugate gradient method, was utilized to minimize the thermal noise and potential energy within the solvated dendrimer structures. Equilibration simulations were carried out for 1 ns under the canonical (NVT) ensemble, maintaining a constant temperature of 310 K using the V-rescale coupling method. A subsequent 1 ns of isothermal-isobaric (NPT) equilibration was performed using the Parrinello-Rahman coupling method to maintain a constant isotropic pressure. Following the equilibration phase, comprehensive 100 ns unrestrained molecular dynamics (MD) simulations were conducted under isothermal-isobaric (NPT) conditions to achieve a fully relaxed and representative state for the solvated dendrimer systems. A 2 fs time step was employed to ensure an accurate capture of the system's dynamics. These meticulously equilibrated dendrimer structures served as the foundation for constructing G4ACE-FA:drug complexes using the blind molecular docking approach facilitated by the AutoDock Vina program [31]. To optimize the docking process, a grid box encompassing the entire G4ACE-FA dendrimer was strategically centered at its center of mass (COM). A grid spacing of 1 Å was implemented to provide a fine-grained resolution for the docking search. Given the absence of experimental data on the simultaneous delivery of 5-FU and SF using G4ACE-FA as a nanocarrier, a sequential molecular docking strategy was adopted. This approach involved utilizing the output of each docking step as the input receptor file for the subsequent docking procedure. The docking process continued iteratively until a significant reduction in the docking scoring function was observed, indicating the identification of energetically favorable binding poses. Specifically, 24 and 25 molecules of 5-FU were docked into the G4ACE-FA dendrimer at physiological and acidic pH conditions, respectively. Furthermore, 11 and 10 molecules of SF were docked under neutral and low pH conditions, respectively. These docking results yielded a final drug loading ratio of G4ACE:5-FU:SF of 1:24:11 at neutral pH and 1:25:10 at low pH. Table 2 provides a detailed overview of the simulated systems, including the overall charge of each system, the number of drug and water molecules, and the number of ions incorporated to maintain physiological ionic strength.

**Table 2**
Details of the simulated systems.

| System | pH | No. docked 5-FU | No. docked SF | No. solvent molecules | No. $Cl^-$ | No. $Na^+$ |
|---|---|---|---|---|---|---|
| **G4ACE-FA** | **Neutral** | – | – | 79047 | 215 | 240 |
| | **Low** | – | – | 78949 | 277 | 215 |
| **G4ACE-FA:5-FU** | **Neutral** | 24 | – | 14120 | 41 | 66 |
| | **Low** | 25 | – | 21705 | 124 | 62 |
| **G4ACE-FA:SF** | **Neutral** | – | 11 | 14031 | 41 | 66 |
| | **Low** | – | 10 | 21641 | 134 | 62 |
| **G4ACE:5-FU:SF** | **Neutral** | 24 | 11 | 13949 | 41 | 66 |
| | **Low** | 25 | 10 | 21517 | 134 | 62 |

## 3. Results and discussion

In the MD simulations of nanocarrier-drug interactions, several common analyses are used to study the behavior and properties of drug molecules, nanocarriers, and their interactions at the atomic level. These analyses provide valuable insights into the dynamics, stability, and binding affinities of drug-loaded nanocarriers, helping researchers

**Table 3**
The radius of gyration ($R_g$) and relaxation time of the unloaded and loaded G4ACE-FA at neutral and low pH conditions.

| | pH | G4ACE-FA | G4ACE-FA:5-FU | G4ACE-FA:SF | G4ACE:5-FU:SF |
|---|---|---|---|---|---|
| ***Rg* (nm)** | **Neutral** | 1.85 ± 0.01 | 1.86 ± 0.01 | 1.83 ± 0.01 | 1.88 ± 0.01 |
| | **Low** | 2.31 ± 0.03 | 2.30 ± 0.03 | 2.32 ± 0.04 | 2.35 ± 0.07 |
| **Relaxation time (ns)** | **Neutral** | 10.2 | 3.4 | 5.0 | 10.4 |
| | **Low** | 9.6 | 7.0 | 5.2 | 9.4 |

optimize drug delivery systems for enhanced efficacy and safety. Some of the common analyses used in MD simulations of nanocarrier-drug interactions include radial distribution function (RDF), root mean square deviation (RMSD), the radius of gyration ($R_g$) and its associated autocorrelation function (ACF), solvent accessible surface area (SASA), and hydrogen bond analysis. These analyses used in MD simulations of nanocarrier-drug interactions provide a comprehensive understanding of the molecular mechanisms governing drug loading, release, and targeting within nanocarrier systems. By employing these analytical tools, researchers can optimize drug delivery systems for improved therapeutic outcomes and advance the development of personalized medicine approaches.

### 3.1. Radius of gyration ($R_g$) and autocorrelation function (ACF)

The $R_g$ and its associated autocorrelation function analyses play a crucial role in characterizing the structural properties, conformational dynamics, and overall behavior of dendrimer molecules. The $R_g$ is a measure of the overall size and compactness of a dendrimer molecule, representing the root mean square distance of its constituent atoms from the center of mass. In MD simulations, calculating the $R_g$ of dendrimers provides insights into their folding, unfolding, and compactness, as well as their response to external forces or environmental changes. By monitoring the $R_g$ values over time, researchers can track structural transitions, assess dendrimer stability, and investigate the impact of different factors on dendrimer conformation. Also, $R_g$ is comparable with previously experimental and theoretical reported results and tells us if the employed FF is reliable. As described previously, all-atom MD simulations were performed on the G4ACE-FA dendrimers and G4ACE-FA:5-FU, G4ACE-FA:SF, and G4ACE-FA:5-FU:SF complexes at physiological and acidic pH conditions to explore the dynamical behavior of loaded and unloaded dendrimers. The $R_g$ for a dendrimer with N atom is calculated as follows:

$$R_g^2 = \frac{1}{M}\sum_{k=1}^{N}\left[m_k(r_k - r_{mean})^2\right] \quad (1)$$

where $M$ is the total mass of the dendrimer, $m_k$ is the mass of the $k$th atom, $r_{mean}$ corresponds to the center of a dendrimer, and $(r_k - r_{mean})$ is the distance of the $k$th atom from the center. Since $R_g$ is a measure of dendrimer size and shape, the equilibrated conformation should fluctuate around a stable average value over time.

It has been observed that the fluctuations in $R_g$ value become insignificant after 50 ns of production MD, indicating that the dendrimer's size and shape remain constant during this time and can be further analyzed. As a result, statistics are collected from the second 50 ns of the MD trajectory. The average $R_g$ value for G4ACE-FA is approximately $1.85 \pm 0.01$ nm and $2.31 \pm 0.03$ nm in physiological and acidic environments, respectively. Table 3 shows that at both neutral and low pH conditions, drug-loading does not appear to significantly affect the size and compactness of G4ACE-FA. A larger dendrimer size is observed when drugs are encapsulated into or conjugated on it, simultaneously. At low pH, the extended structure of the dendrimer is due to repulsion between positively charged branching monomers, resulting in numerous cavities.

The equilibration of simulated systems was determined using the autocorrelation function of $R_g$ as a function of simulation time ($C_{R_g}(t)$), which can be expressed using the following equation:

$$C_{R_g}(t) = \frac{\langle\left(R_g^2(t) - \langle R_g^2\rangle\right)\left(R_g^2(0) - \langle R_g^2\rangle\right)\rangle}{\langle R_g^4\rangle - \langle R_g^2\rangle^2} \quad (2)$$

The autocorrelation function is a mathematical tool used to analyze the temporal correlation of a property or variable within a system. In the context of MD simulations of dendrimers, autocorrelation functions are often applied to study the dynamical behavior of specific structural parameters, such as $R_g$, end-to-end distance, or internal motions. By calculating the autocorrelation function of $R_g$, researchers can quantify the persistence of structural fluctuations, characterize the timescales of dendrimer motion, and identify patterns of correlated movements within the dendrimer structure. We analyze the equilibration rate of G4ACE-FA at two distinct environmental pH levels by examining the relaxation time parameter. The relaxation time represents the duration required for a disturbed system to return to equilibrium, defined as the point when $C_{R_g}(t) = 1/e$. The relaxation times for G4ACE-FA at neutral and low pH are calculated to be 10.2 and 9.6 ns, respectively. This suggests that G4ACE-FA achieves equilibrium at a similar rate under both pH conditions. This phenomenon may be attributed to the initial extended structures of G4ACE-FA at both low and neutral pH resembling a starburst configuration, facilitating the monomers of the dendrimers to reorganize into a stable architecture within a reasonable timeframe. The shortest relaxation times are observed when G4ACE-FA interacts with 5-FU molecules. The incorporation of small 5-FU drug molecules does not significantly alter the microstructure of the dendrimer. These drug molecules can freely move within the simulation box and integrate into the dendrimer with minimal changes to its microstructure. The doubling

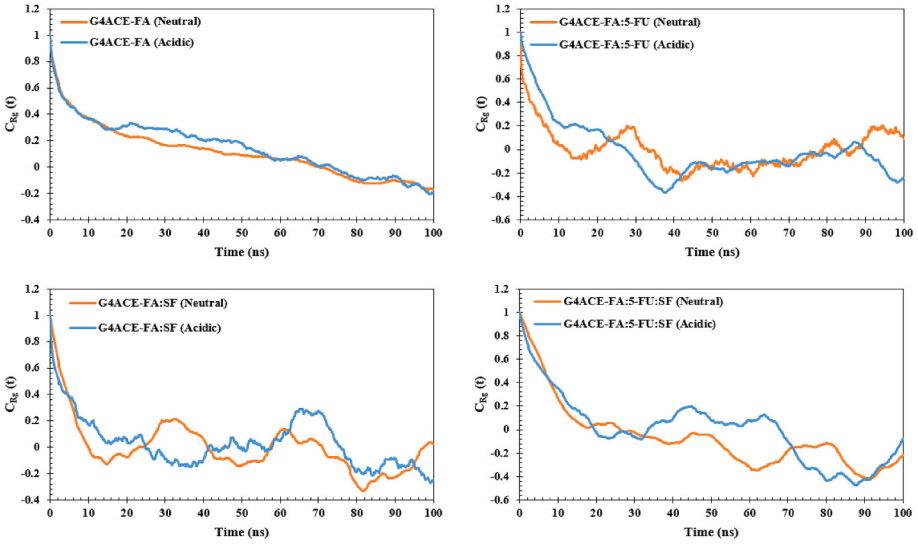


**Fig. 1.** Autocorrelation function of the $R_g$ as a function of time $C_{R_g}(t)$ for unloaded and loaded G4ACE-FA at neutral and low pH conditions.

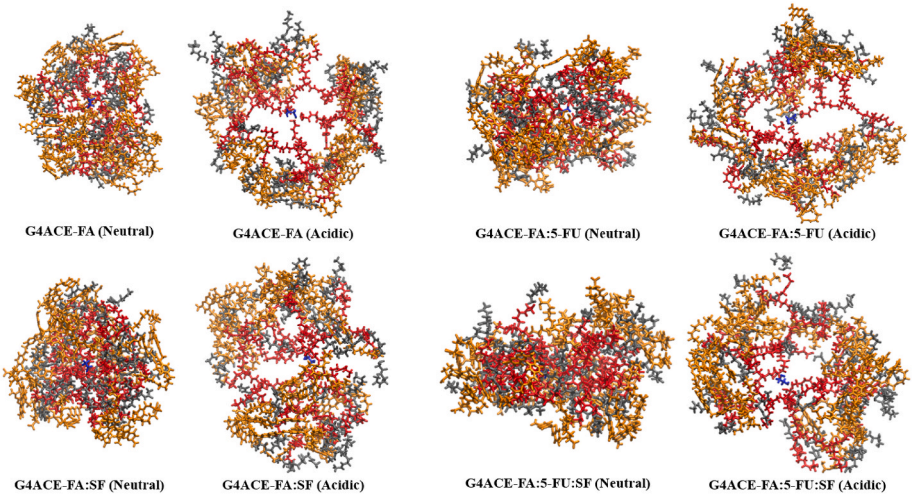


**Fig. 2.** Equilibrium conformations of unloaded and loaded G4ACE-FA at neutral and acidic environments. Atoms are represented using licorice cylinders. Solvent, drugs, and electrolyte ions have been hidden for more clarity. The ethylene diamine core is shown in blue, internal monomers are in red, acetyl-terminated monomers are in gray, and FA residues are in orange.

**Table 4**
Average values of the aspect ratios and asphericity of unloaded and loaded G4ACE-FA at different pH conditions.

| System | pH | Principal moments of inertia | | | Aspect ratios | | asphericity |
|---|---|---|---|---|---|---|---|
| | | $I_x$ | $I_y$ | $I_z$ | $I_z/I_y$ | $I_z/I_x$ | δ |
| **G4ACE-FA** | **Neutral** | 45.3 ± 1.7 | 62.7 ± 2.8 | 74.0 ± 2.1 | 1.2 ± 0.03 | 1.6 ± 0.1 | 0.02 |
| | **Low** | 70.6 ± 4.1 | 96.2 ± 6.4 | 118.3 ± 6.8 | 1.2 ± 0.06 | 1.7 ± 0.1 | 0.02 |
| **G4ACE-FA:5-FU** | **Neutral** | 50.0 ± 1.2 | 58.8 ± 2.1 | 75.4 ± 1.4 | 1.3 ± 0.04 | 1.5 ± 0.05 | 0.01 |
| | **Low** | 69.3 ± 3.9 | 90.8 ± 4.6 | 119.2 ± 5.4 | 1.3 ± 0.05 | 1.7 ± 0.1 | 0.02 |
| **G4ACE-FA:SF** | **Neutral** | 45.9 ± 1.0 | 62.4 ± 1.1 | 70.2 ± 1.0 | 1.1 ± 0.02 | 1.5 ± 0.03 | 0.01 |
| | **Low** | 70.1 ± 3.5 | 94.1 ± 4.9 | 119.5 ± 5.9 | 1.3 ± 0.05 | 1.7 ± 0.1 | 0.03 |
| **G4ACE-FA:5-FU:SF** | **Neutral** | 46.5 ± 1.2 | 64.7 ± 1.0 | 75.8 ± 1.1 | 1.2 ± 0.02 | 1.6 ± 0.05 | 0.02 |
| | **Low** | 71.2 ± 3.8 | 96.8 ± 4.5 | 119.8 ± 2.9 | 1.2 ± 0.05 | 1.7 ± 0.1 | 0.02 |

of the relaxation time in acidic pH can be elucidated by the fact that in neutral pH, the dendrimer possesses a tightly compact structure, making it challenging for drug molecules to infiltrate. Conversely, in acidic pH, the interaction of the dendrimer with molecules through the monomers of the inner layers leads to continuous intrastructural modifications, delaying equilibrium attainment. The prolonged relaxation time in G4ACE-FA:5-FU: SF is legitimized by the competition among 5-FU and SF drug molecules to be encapsulated by the dendrimer when interacting simultaneously. Fig. 1 illustrates that the autocorrelation function of G4ACE-FA fluctuates around zero during the last 50 ns of the simulation period, affirming the reliability of selecting statistics from this timeframe in the MD trajectory.

The unloaded and loaded structures of G4ACE-FA at different environmental pH conditions show that it adopts a densely packed conformation at neutral pH but possesses an open and sponge-like structure at low pH (Fig. 2).

Principal moments of inertia ($I_z$, $I_y$, and $I_x$ in descending order) analysis was conducted to evaluate the shape of G4ACE-FA under varying simulation conditions. The moment of inertia-based aspect ratios of $I_z/I_y$ and $I_z/I_x$ were utilized to determine the geometric shape of the dendrimers in terms of either ellipsoidal or spherical shapes. Additionally, we calculated the asphericity values ($\delta$) using the following formula:

$$\delta = 1 - 3\frac{\langle I_2 \rangle}{\langle I_1^2 \rangle} \tag{3}$$

where $I_1$ and $I_2$ are the first and second invariants of the $R_g$ tensor, respectively:

$$I_1 = I_x + I_y + I_z \tag{4}$$

$$I_2 = I_x I_y + I_y I_z + I_x I_z \tag{5}$$

When the aspect ratios and asphericity value of a molecule are equal to 1 and 0 respectively, it is considered a perfect sphere. Any deviation from these values results in a more elliptical shape of the molecule.

As the data in Table 4 shows, the values of aspect ratios and asphericity deviate to some extent from 1 to 0, which indicates a slight deviation from the completely spherical structure. The highest level of asphericity is related to the G4ACE-FA: SF structure, which is also confirmed by Fig. 2.

### 3.2. Solvent accessible surface area (SASA) analysis

Surface area accessible to solvent molecules, also known as solvent accessible surface area (SASA), is a measure of the surface area of a molecule that is open to solvent molecules. In dendrimers, calculating the SASA involves determining the surface area of the dendrimer that is not covered by other atoms within a specified probe radius, typically representing the size of a water molecule. By quantifying the SASA of different parts of the dendrimer structure, researchers can assess the degree of exposure of specific functional groups, binding sites, or hydrophobic regions to the surrounding solvent, providing insights into their accessibility and potential roles in molecular interactions. SASA analysis can reveal how dendrimer molecules interact with solvent molecules, identifying regions that are more or less exposed to the surrounding environment. Variations in SASA values over time can indicate changes in solvation patterns, hydration dynamics, or solvent

**Table 5**
Average COM separation distance (in nm) between dendrimers and the drug molecules (5-FU and SF).

| 5-FU | G4ACE-FA:5-FU | | G4ACE-FA:5-FU:SF | | SF | G4ACE-FA:SF | | G4ACE-FA:5-FU:SF | |
|---|---|---|---|---|---|---|---|---|---|
| | Neutral | Low | Neutral | Low | | Neutral | Low | Neutral | Low |
| $R_g$ | 1.9 ± 0.01 | 2.3 ± 0.03 | 1.9 ± 0.01 | 2.4 ± 0.07 | | 1.8 ± 0.01 | 2.3 ± 0.04 | 1.9 ± 0.01 | 2.4 ± 0.07 |
| **5-FU 1** | 0.9 ± 0.04 | 2.0 ± 0.2 | 2.3 ± 0.05 | 2.3 ± 0.05 | **SF 1** | 1.2 ± 0.06 | 1.5 ± 0.1 | 1.4 ± 0.05 | 2.4 ± 0.1 |
| **5-FU 2** | 0.9 ± 0.05 | 3.8 ± 1.3 | 1.6 ± 0.09 | 3.6 ± 1.0 | **SF 2** | 1.1 ± 0.03 | 1.7 ± 0.2 | 1.2 ± 0.03 | 1.6 ± 0.02 |
| **5-FU 3** | 0.9 ± 0.03 | 3.9 ± 1.0 | 1.9 ± 0.1 | 3.8 ± 1.1 | **SF 3** | 1.9 ± 0.06 | 2.9 ± 0.4 | 2.1 ± 0.01 | 3.2 ± 0.4 |
| **5-FU 4** | 2.4 ± 0.08 | 3.5 ± 1.2 | 2.2 ± 0.05 | 3.2 ± 0.9 | **SF 4** | 1.5 ± 0.05 | 3.1 ± 0.3 | 1.3 ± 0.06 | 3.6 ± 1.3 |
| **5-FU 5** | 2.5 ± 0.8 | 2.0 ± 0.1 | 2.7 ± 0.7 | 2.1 ± 0.08 | **SF 5** | 1.4 ± 0.03 | 2.8 ± 0.4 | 1.4 ± 0.05 | 2.8 ± 1.4 |
| **5-FU 6** | 2.6 ± 0.9 | 3.9 ± 1.0 | 2.1 ± 0.7 | 3.7 ± 1.0 | **SF 6** | 1.2 ± 0.04 | 3.0 ± 0.2 | 1.5 ± 0.09 | 3.5 ± 1.2 |
| **5-FU 7** | 3.3 ± 0.9 | 2.7 ± 1.4 | 2.3 ± 0.3 | 3.7 ± 0.06 | **SF 7** | 1.6 ± 0.05 | 2.5 ± 0.01 | 1.8 ± 0.1 | 2.3 ± 0.08 |
| **5-FU 8** | 0.9 ± 0.1 | 2.8 ± 0.8 | 2.0 ± 0.06 | 3.2 ± 0.9 | **SF 8** | 1.6 ± 0.04 | 2.6 ± 0.3 | 1.9 ± 0.08 | 2.6 ± 1.1 |
| **5-FU 9** | 3.0 ± 0.8 | 3.2 ± 1.4 | 2.8 ± 0.9 | 3.6 ± 1.2 | **SF 9** | 2.2 ± 0.06 | 2.0 ± 0.3 | 2.0 ± 1.4 | 2.9 ± 0.3 |
| **5-FU 10** | 2.7 ± 0.8 | 2.3 ± 0.09 | 0.9 ± 0.03 | 2.0 ± 0.1 | **SF 10** | 1.3 ± 0.03 | 2.8 ± 0.6 | 1.6 ± 0.09 | 2.9 ± 0.9 |
| **5-FU 11** | 2.0 ± 0.09 | 3.7 ± 1.0 | 2.8 ± 1.0 | 3.3 ± 1.1 | **SF 11** | 1.7 ± 0.1 | – | 1.8 ± 0.1 | – |
| **5-FU 12** | 3.2 ± 1.0 | 3.7 ± 1.3 | 1.0 ± 0.1 | 2.9 ± 1.2 | | | | | |
| **5-FU 13** | 0.9 ± 0.05 | 3.6 ± 1.3 | 2.0 ± 0.03 | 3.6 ± 1.0 | | | | | |
| **5-FU 14** | 2.9 ± 1.2 | 3.2 ± 0.9 | 2.0 ± 1.1 | 3.4 ± 0.5 | | | | | |
| **5-FU 15** | 2.1 ± 0.01 | 3.8 ± 0.9 | 3.0 ± 0.8 | 2.8 ± 1.4 | | | | | |
| **5-FU 16** | 3.3 ± 1.2 | 3.2 ± 1.0 | 2.7 ± 0.5 | 3.5 ± 1.0 | | | | | |
| **5-FU 17** | 2.8 ± 1.2 | 2.6 ± 0.9 | 2.8 ± 1.2 | 3.6 ± 0.8 | | | | | |
| **5-FU 18** | 2.3 ± 0.07 | 3.7 ± 1.3 | 2.4 ± 0.9 | 3.2 ± 1.4 | | | | | |
| **5-FU 19** | 1.4 ± 0.1 | 3.2 ± 1.1 | 1.5 ± 0.05 | 3.6 ± 0.7 | | | | | |
| **5-FU 20** | 3.2 ± 0.8 | 2.9 ± 0.6 | 2.4 ± 0.5 | 2.9 ± 0.4 | | | | | |
| **5-FU 21** | 2.7 ± 1.2 | 3.9 ± 1.2 | 1.8 ± 0.06 | 3.1 ± 1.3 | | | | | |
| **5-FU 22** | 3.0 ± 1.3 | 3.9 ± 1.1 | 2.3 ± 0.1 | 2.9 ± 1.2 | | | | | |
| **5-FU 23** | 2.1 ± 0.04 | 3.7 ± 1.0 | 2.9 ± 1.0 | 3.5 ± 1.0 | | | | | |
| **5-FU 24** | 3.2 ± 1.2 | 3.5 ± 1.3 | 2.6 ± 0.9 | 3.5 ± 0.4 | | | | | |
| **5-FU 24** | – | 3.7 ± 1.1 | | 3.2 ± 1.3 | | | | | |

**Table 6**
Calculated stoichiometries for dendrimer:drug complexes obtained from the analysis of COM separation distance between dendrimer and drug molecules during the last 50 ns of MD simulations.

| Complex | pH | Drug | Initial stoichiometry | Equilibrium stoichiometry | Internally complexed drugs | Externally complexed drugs |
|---|---|---|---|---|---|---|
| **G4ACE-FA:5-FU** | **Neutral** | **5-FU** | 1:24 | 1:11 | 6 | 5 |
| | **Low** | | 1:25 | 1:3 | 0 | 3 |
| **G4ACE-FA:SF** | **Neutral** | **SF** | 1:11 | 1:10 | 6 | 4 |
| | **Low** | | 1:10 | 1:4 | 2 | 2 |
| **G4ACE-FA:5-FU:SF** | **Neutral** | **5-FU** | 1:24 | 1:11 | 4 | 7 |
| | **Low** | | 1:25 | 1:3 | 0 | 3 |
| | **Neutral** | **SF** | 1:11 | 1:10 | 6 | 4 |
| | **Low** | | 1:10 | 1:3 | 1 | 2 |

penetration into the dendrimer structure. By analyzing the SASA values of specific functional groups or binding sites on the dendrimer surface, researchers can identify potential interaction sites for ligands, substrates, or other molecules. Changes in SASA can indicate the formation or disruption of binding interactions, guiding the study of molecular recognition and complex formation processes. Monitoring SASA values during molecular dynamics (MD) simulations can help track conformational changes in molecule structures, such as unfolding events, surface fluctuations, or domain rearrangements. Differences in SASA between different simulation conditions or molecule variants can highlight structural flexibility and stability differences. Overall, SASA analysis provides valuable information about the solvation behavior, surface properties, and potential interaction sites of dendrimers in MD simulations. By combining SASA calculations with other structural analyses such as radius of gyration and autocorrelation functions, researchers can gain a comprehensive understanding of dendrimer behavior at the molecular level, facilitating the design and optimization of dendrimer-based materials, drug delivery systems, and nanotechnologies. At neutral pH, the calculated values of SASA are about 124.0 ± 2.8, 127.5 ± 2.6, 131.3 ± 2.6, and 133.3 ± 2.6 $nm^2$ for the unloaded G4ACE-FA, and dendrimer in G4ACE-FA:5-FU, G4ACE-FA:SF, and G4ACE-FA:5-FU:SF complexes, respectively. Drug loading does not have a significant impact on the SASA of dendrimers. The corresponding values at low pH are 198.2 ± 4.7, 195.8 ± 4.8, 212.5 ± 6.1, and 215.4 ± 4.2 $nm^2$. From this data, we conclude that the incorporation of 5-FU has minimal impact on the exposure of the dendrimer surface to solvent molecules, indicating that 5-FU encapsulation occurs with slight changes in the microstructure of the dendrimer. This could be attributed to the small size of this drug molecule. However, when the dendrimer interacts with SF molecules, a more pronounced increase in the SASA values is observed, indicating an expansion of the dendrimer's structure for conjugation with SF drug molecules.

### 3.3. Loading capacity of G4ACE-FA

The initial assessment of G4ACE-FA:drug(s) was accomplished through a sequential molecular docking approach as previously described. To gain more detailed insights into the atomic microstructure and stability of the G4ACE-FA:drug(s) complexes, as well as the dendrimer's drug loading capacity at various pH values and preferential binding sites of bound 5-FU and SF molecules, all-atom molecular dynamics (MD) simulations were conducted for 100 ns. The criterion for selecting a drug molecule as part of a stable complex was based on the center of mass (COM) separation distance between the drug molecule and dendrimer being almost equal to or less than the value of $R_g$. If the molecule met this criterion, it was considered a part of the carrier-cargo

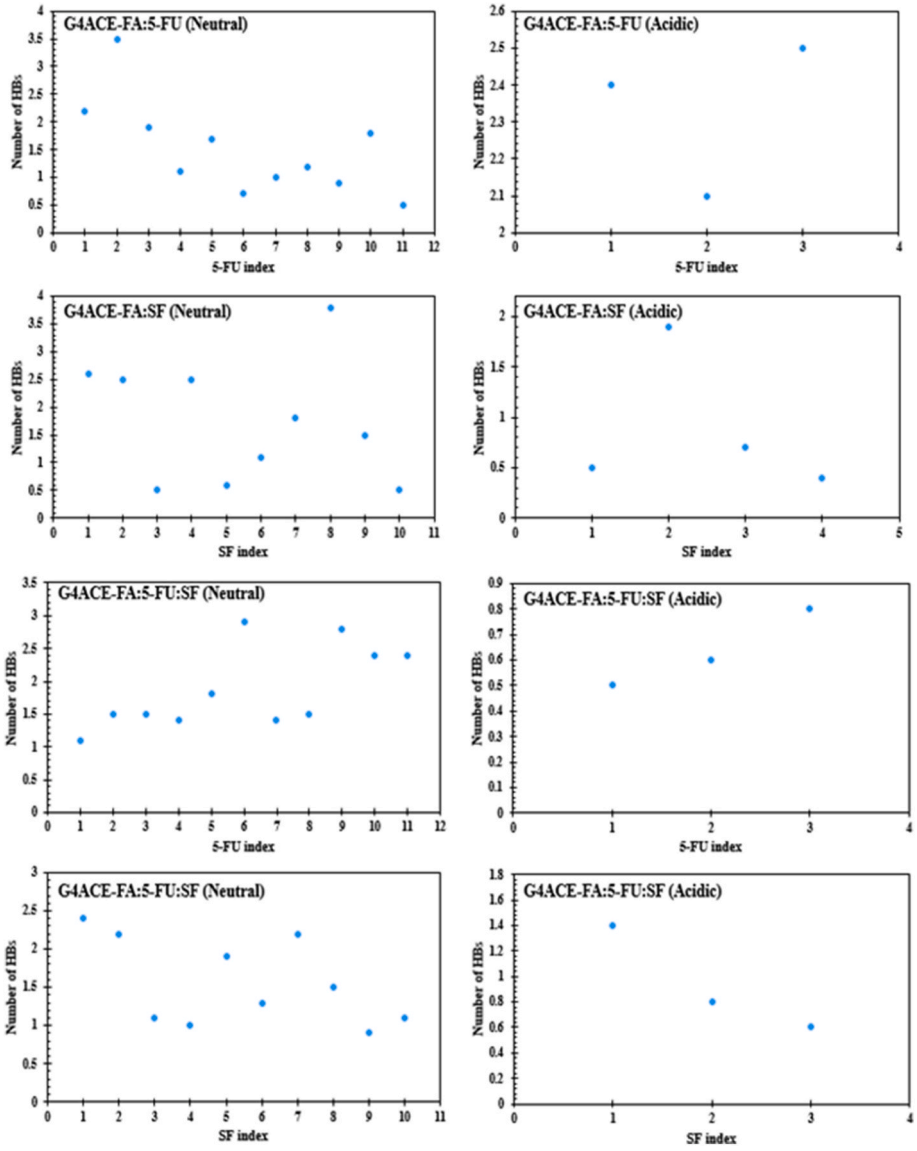


**Fig. 3.** The average number of HBs formed between the dendrimer and drugs at various environmental conditions.

complex. The MD simulations revealed that the equilibrium stoichiometry of the G4ACE-FA:5-FU complex was 1:11 and 1:3 at neutral and low pH, respectively. In the case of the G4ACE-FA:SF complex, the equilibrium stoichiometry was found to be 1:10 and 1:4 at neutral and low pH conditions, respectively. The G4ACE-FA:5-FU:SF complex had a stoichiometry of 1:11:10 at neutral pH and 1:3:3 at low pH. The significant decrease in drug loading at acidic pH suggests that G4ACE-FA can serve as a convenient nanovector that can tightly bind drug molecules at neutral pH and release them at tumor cells, thus facilitating targeted drug delivery. Additionally, the co-loading of 5-FU and SF did not diminish the loading capacity of G4ACE-FA, which is an interesting observation.

Having information about the preferred binding site of drug molecules is of particular importance in the field of targeted drug delivery because it provides a measure of the rate at which drug molecules are released. The more molecules of the drug are located in the interior layers of the dendrimer, the slower and more continuous the release, which is more desirable from a drug delivery perspective. Table 5 shows the average COM separation distance between G4ACE-FA and the bound drug molecules at neutral pH during the last 50 ns of MD trajectories, which guarantees the equilibrium behavior of the simulated systems. In the G4ACE-FA:5-FU complex and at neutral pH drug molecules are distributed evenly on the surface and into the cavities of dendrimer so that 6 drug molecules are entrapped in the interior layers, while 5 of them are conjugated on the surface of the dendrimer. At low pH, all 3 bound drugs are located on the periphery of the dendrimer. In the G4ACE-FA:SF complex and at neutral pH 6 drug molecules are entrapped in the interior layers, while 4 of them are conjugated on the surface of the dendrimer. At low pH 2 SF molecules are located on the surface of G4ACE-FA, while 2 other SF molecules are internally complexed within the dendrimer. The preferential binding sites of 5-FU and SF molecules in G4ACE-FA:5-FU:SF complex at both physiological and cancerous environments are represented in Table 6.

### 3.4. Hydrogen bonds (HBs) analysis

Hydrogen bonds (HBs) play a crucial role in stabilizing molecular structures within nanocarrier-drug systems during MD simulations. Analyzing HBs provides valuable insights into the intermolecular interactions and dynamics of these systems. Understanding HB formation and disruption helps in predicting the stability and drug release kinetics of nanocarrier-drug complexes. HB analysis can also aid in optimizing the design of nanocarriers for efficient drug delivery by identifying key interactions between the carrier and drug molecules. Moreover,

studying hydrogen bonds in MD simulations allows researchers to investigate the binding affinity and specificity of drugs to nanocarriers, which is essential for developing targeted and effective drug delivery systems. Therefore, we performed HBs analysis to investigate the number of HBs formed between the dendrimer and drug molecules and to explore the interacting residues and atoms. It can be seen from Fig. 3 that the number of HBs decreases to some extent at low pH, which is favorable from a drug delivery viewpoint and may facilitate drug release. The analyses showed that the FA residues are involved in HB interactions with the drug molecules, indicating their importance in the stabilization of the nanocarrier:drug complexes. The results of this study are consistent with earlier research. It seems that combining folic acid with other functional groups doesn't significantly affect the size of nanocarriers, but it does affect how much they can hold in different environmental settings. Both this study and previous ones suggest that folic acid can help target the delivery of drugs (see Table 1 for more details) [1–3,7,8,13].

## 4. Conclusion

Molecular dynamics (MD) simulations were conducted to investigate the simultaneous association of sorafenib (SF) and 5-fluorouracil (5-FU) drug molecules with folic acid-conjugated and acetyl-terminated poly (amidoamine) (PAMAM) dendrimers of generation 4 (G4ACE-FA). The simulations were performed under physiological (pH = 7.4) and low (pH < 5) pH conditions, which represent healthy and tumor cells, respectively. The incorporation of drugs did not appear to have a significant impact on the size and compactness of G4ACE-FA under both neutral and low pH conditions. However, a larger dendrimer size was observed when drugs were encapsulated into or conjugated on it simultaneously. At low pH, the extended structure of the dendrimer is due to repulsion between positively charged branching monomers, resulting in numerous cavities. The unloaded and loaded structures of G4ACE-FA at different environmental pH conditions demonstrated that it adopts a densely packed conformation at neutral pH but possesses an open and sponge-like structure at low pH. The values of aspect ratios and asphericity deviate slightly from 1 to 0, respectively, indicating a slight deviation from the completely spherical structure. The highest level of asphericity was observed in the G4ACE-FA:SF structure. At neutral pH, the calculated values of surface area to volume ratio (SASA) were found to be about $124.0 \pm 2.8$, $127.5 \pm 2.6$, $131.3 \pm 2.6$, and $133.3 \pm 2.6$ $nm^2$ for the unloaded G4ACE-FA, and dendrimer in G4ACE-FA:5-FU, G4ACE-FA:SF, and G4ACE-FA:5-FU:SF complexes, respectively. The incorporation of drugs did not have a significant impact on the SASA of dendrimers. The corresponding values at low pH were $198.2 \pm 4.7$, $195.8 \pm 4.8$, $212.5 \pm 6.1$, and $215.4 \pm 4.2$ $nm^2$. From this data, we can conclude that the incorporation of 5-FU has minimal impact on the exposure of the dendrimer surface to solvent molecules, indicating that 5-FU encapsulation occurs with slight changes in the microstructure of the dendrimer. This could be attributed to the small size of this drug molecule. However, when the dendrimer interacts with SF molecules, a more pronounced increase in the SASA values is observed, indicating an expansion of the dendrimer's structure for conjugation with SF drug molecules. The MD simulations revealed that the equilibrium stoichiometry of the G4ACE-FA:5-FU complex was 1:11 and 1:3 at neutral and low pH, respectively. In the case of the G4ACE-FA:SF complex, the equilibrium stoichiometry was found to be 1:10 and 1:4 at neutral and low pH conditions, respectively. The G4ACE-FA:5-FU:SF complex had a stoichiometry of 1:11:10 at neutral pH and 1:3:3 at low pH. The significant decrease in drug loading at acidic pH suggests that G4ACE-FA can serve as a convenient nanovector that can tightly bind drug molecules at neutral pH and release them at tumor cells, thus facilitating targeted drug delivery. Additionally, the co-loading of 5-FU and SF did not diminish the loading capacity of G4ACE-FA, which is an interesting observation. In the G4ACE-FA:5-FU complex and at neutral pH, drug molecules were distributed evenly on the surface and into the cavities of the dendrimer, with 6 drug molecules entrapped in the interior layers and 5 of them conjugated on the surface of the dendrimer. At low pH, all three bound drugs were located on the periphery of the dendrimer. In the G4ACE-FA:SF complex and at neutral pH, 6 drug molecules were entrapped in the interior layers, and 4 of them were conjugated on the surface of the dendrimer. At low pH, 2 SF molecules were located on the surface of G4ACE-FA, while 2 other SF molecules were internally complexed within the dendrimer. The preferential binding sites of 5-FU and SF did not change considerably when they were complexed simultaneously to the G4ACE-FA dendrimer. Thus, co-delivery of 5-FU and SF using G4ACE-FA dendrimer seems to be a strategic approach for improving the efficiency of these chemotherapeutics.

## CRediT authorship contribution statement

**Ali Hussein Mezher:** Software, Methodology, Data curation, Conceptualization. **Mahboobeh Salehpour:** Writing – review & editing, Writing – original draft, Visualization, Validation, Supervision, Resources, Project administration, Methodology, Investigation, Funding acquisition, Formal analysis, Data curation, Conceptualization. **Zohreh Saadati:** Writing – review & editing, Writing – original draft, Visualization, Validation, Supervision, Resources, Project administration, Methodology, Investigation, Funding acquisition, Formal analysis, Data curation, Conceptualization.

## Data availability

Data will be made available on request.

## References

[1] F. Badalkhani-Khamseh, A. Ebrahim-Habibi, N.L. Hadipour, Atomistic computer simulations on multi-loaded PAMAM dendrimers: a comparison of amine-and hydroxyl-terminated dendrimers, J. Comput. Aided Mol. Des. 31 (2017) 1097–1111.
[2] F. Badalkhani-Khamseh, A. Ebrahim-Habibi, N.L. Hadipour, Influence of dendrimer surface chemistry and pH on the binding and release pattern of chalcone studied by molecular dynamics simulations, J. Mol. Recogn. 32 (2019) e2757.
[3] C.-k. Tu, W. Mou, Z.-L. Shen, Computer simulation of the structural properties of fatty-acid modified PAMAM dendrimers at pH 5 and 7, J. Mol. Graph. Model. 124 (2023) 108570.
[4] P. Tagde, G.T. Kulkarni, D.K. Mishra, P. Kesharwani, Recent advances in folic acid engineered nanocarriers for treatment of breast cancer, J. Drug Deliv. Sci. Technol. 56 (2020) 101613.
[5] H. Choudhury, M. Pandey, L.P. Wen, L.K. Cien, H. Xin, A.N. Yee, et al., Folic acid conjugated nanocarriers for efficient targetability and promising anticancer efficacy for treatment of breast cancer: a review of recent updates, Curr. Pharmaceut. Des. 26 (2020) 5365–5379.
[6] B. Bahrami, M. Mohammadnia-Afrouzi, P. Bakhshaei, Y. Yazdani, G. Ghalamfarsa, M. Yousefi, et al., Folate-conjugated nanoparticles as a potent therapeutic approach in targeted cancer therapy, Tumor Biol. 36 (2015) 5727–5742.
[7] S. Ullah, A.K. Azad, A. Nawaz, K.U. Shah, M. Iqbal, G.M. Albadrani, et al., 5-fluorouracil-loaded folic-acid-fabricated chitosan nanoparticles for site-targeted drug delivery cargo, Polymers 14 (2022) 2010.
[8] G. Birlik Demirel, E. Aygul, A. Dag, S. Atasoy, Z. Cimen, B. Cetin, Folic acid-conjugated pH and redox-sensitive ellipsoidal hybrid magnetic nanoparticles for dual-triggered drug release, ACS Appl. Bio Mater. 3 (2020) 4949–4961.
[9] M. Yahyavi, F. Badalkhani-Khamseh, N.L. Hadipour, Adsorption behavior of pristine, Al-, and Si-doped carbon nanotubes upon 5-fluorouracil, Chem. Phys. Lett. 750 (2020) 137492.
[10] U. Sahebi, H. Gholami, B. Ghalandari, F. Badalkhani-khamseh, A. Nikzamir, A. Divsalar, Evaluation of BLG ability for binding to 5-FU and Irinotecan simultaneously under acidic condition: a spectroscopic, molecular docking and molecular dynamic simulation study, J. Mol. Liq. 344 (2021) 117758.
[11] R. Esfandiarpour, F. Badalkhani-Khamseh, N.L. Hadipour, Theoretical studies of phosphorene as a drug delivery nanocarrier for fluorouracil, RSC Adv. 13 (2023) 18058–18069.
[12] S. Blondy, V. David, M. Verdier, M. Mathonnet, A. Perraud, N. Christou, 5-Fluorouracil resistance mechanisms in colorectal cancer: from classical pathways to promising processes, Cancer Sci. 111 (2020) 3142–3154.
[13] M. Yahyavi, F. Badalkhani-Khamseh, N.L. Hadipour, Folic acid functionalized carbon nanotubes as pH controlled carriers of fluorouracil: molecular dynamics simulations, J. Mol. Liq. 377 (2023) 121393.
[14] B. Escudier, F. Worden, M. Kudo, Sorafenib: key lessons from over 10 years of experience, Expet Rev. Anticancer Ther. 19 (2019) 177–189.

[15] J.-L. Raoul, M. Kudo, R.S. Finn, J. Edeline, M. Reig, P.R. Galle, Systemic therapy for intermediate and advanced hepatocellular carcinoma: sorafenib and beyond, Cancer Treat Rev. 68 (2018) 16–24.
[16] R. Dennington, T. Keith, J. Millam, GaussView, Version 5, 2009.
[17] V. Hornak, R. Abel, A. Okur, B. Strockbine, A. Roitberg, C. Simmerling, Comparison of multiple Amber force fields and development of improved protein backbone parameters, Proteins: Struct., Funct., Bioinf. 65 (2006) 712–725.
[18] M. Frisch, G. Trucks, H. Schlegel, G. Scuseria, M. Robb, J. Cheeseman, et al., Gaussian 09, Revision a. 02; Gaussian, Inc: Wallingford, Ct, 2009. Google Scholar There Is No Corresponding Record for This Reference, 2015.
[19] E. Vanquelef, S. Simon, G. Marquant, E. Garcia, G. Klimerak, J.C. Delepine, et al., RED Server: a web service for deriving RESP and ESP charges and building force field libraries for new molecules and molecular fragments, Nucleic Acids Res. 39 (2011) W511–W517.
[20] C. Diaz, C. Benitez, F. Vidal, L.F. Barraza, V.A. Jiménez, L. Guzman, et al., Cytotoxicity and in vivo plasma kinetic behavior of surface-functionalized PAMAM dendrimers, Nanomed. Nanotechnol. Biol. Med. 14 (2018) 2227–2234.
[21] J. Wang, W. Wang, P.A. Kollman, D.A. Case, Antechamber: an accessory software package for molecular mechanical calculations, J. Am. Chem. Soc. 222 (2001).
[22] A.W. Sousa da Silva, W.F. Vranken, ACPYPE-Antechamber python parser interface, BMC Res. Notes 5 (2012) 1–8.
[23] D. Van Der Spoel, E. Lindahl, B. Hess, G. Groenhof, A.E. Mark, H.J. Berendsen, GROMACS: fast, flexible, and free, J. Comput. Chem. 26 (2005) 1701–1718.
[24] W. Humphrey, A. Dalke, K. Schulten, VMD: visual molecular dynamics, J. Mol. Graph. 14 (1996) 33–38.
[25] D. Cakara, J. Kleimann, M. Borkovec, Microscopic protonation equilibria of poly (amidoamine) dendrimers from macroscopic titrations, Macromolecules 36 (2003) 4201–4207.
[26] Y. Niu, L. Sun, R.M. Crooks, Determination of the intrinsic proton binding constants for poly (amidoamine) dendrimers via potentiometric pH titration, Macromolecules 36 (2003) 5725–5731.
[27] M.S. Diallo, S. Christie, P. Swaminathan, L. Balogh, X. Shi, W. Um, et al., Dendritic chelating agents. 1. Cu (II) binding to ethylene diamine core poly (amidoamine) dendrimers in aqueous solutions, Langmuir 20 (2004) 2640–2651.
[28] S. Pande, R.M. Crooks, Analysis of poly (amidoamine) dendrimer structure by UV–Vis spectroscopy, Langmuir 27 (2011) 9609–9613.
[29] K. Mioduszewska, J. Dołżonek, D. Wyrzykowski, Ł. Kubik, P. Wiczling, C. Sikorska, et al., Overview of experimental and computational methods for the determination of the pKa values of 5-fluorouracil, cyclophosphamide, ifosfamide, imatinib and methotrexate, TrAC, Trends Anal. Chem. 97 (2017) 283–296.
[30] J. Wielińska, A. Nowacki, B. Liberek, 5-fluorouracil—complete insight into its neutral and ionised forms, Molecules 24 (2019) 3683.
[31] O. Trott, A.J. Olson, AutoDock Vina: improving the speed and accuracy of docking with a new scoring function, efficient optimization, and multithreading, J. Comput. Chem. 31 (2010) 455–461.